Cellular/Molecular

P/Q and N Channels Control Baseline and Spike-Triggered Calcium Levels in Neocortical Axons and Synaptic Boutons

Yuguo Yu,* Carlos Maureira,* Xiuxin Liu, and David McCormick
Department of Neurobiology, Kavli Institute for Neuroscience, Yale University School of Medicine, New Haven, Connecticut 06520

Cortical axons contain a diverse range of voltage-activated ion channels, including Ca^{2+} currents. Interestingly, Ca^{2+} channels are not only located at presynaptic terminals, but also in the axon initial segment (AIS), suggesting a potentially important role in the regulation of action potential generation and neuronal excitability. Here, using two-photon microscopy and whole-cell patch-clamp recording, we examined the properties and role of calcium channels located in the AIS and presynaptic terminals of ferret layer 5 prefrontal cortical pyramidal cells *in vitro*. Subthreshold depolarization of the soma resulted in an increase in baseline and spike-triggered calcium concentration in both the AIS and nearby synaptic terminals. The increase in baseline calcium concentration rose with depolarization and fell with hyperpolarization with a time constant of approximately 1 s and was blocked by removal of Ca^{2+} from the bathing medium. The increases in calcium concentration at the AIS evoked by subthreshold or suprathreshold depolarization of the soma were blocked by the P/Q-channel antagonist ω-agatoxin IVA or the N-channel antagonist ω-conotoxin GVIA or both. The presence of these channels in the AIS pyramidal cells was confirmed with immunochemistry. Block of these channels slowed axonal action potential repolarization, apparently from reduction of the activation of a Ca^{2+}-activated K^+ current, and increased neuronal excitability. These results demonstrate novel mechanisms by which calcium currents may control the electrophysiological properties of axonal spike generation and neurotransmitter release in the neocortex.

Introduction

Axons are electrophysiologically and anatomically unique structures that perform a variety of functions including the integration of synaptic signals and initiation of action potentials (Magee et al., 1995; Debanne, 2004; Alle and Geiger, 2006; Shu et al., 2006a, 2007a,b; Kole et al., 2007, 2008), conduction of both subthreshold and suprathreshold waveforms into local axon branches (Alle and Geiger, 2006; Shu et al., 2006a; Kole et al., 2007), and presynaptic transmitter release, at times in a mixed digital-and-analog manner (Awatramani et al., 2005; Alle and Geiger, 2006; Shu et al., 2006a). It now appears that many of the electrophysiological properties that were once attributed to the soma and/or dendrites may be complemented and/or mediated by a unique mixture of ionic currents present in the axon initial segment (AIS) (Stuart et al., 1997; Debanne, 2004; Astman et al., 2006; Kole et al., 2007; Shu et al., 2007a,b; Yu et al., 2008; Hu et al., 2009).

Immunocytochemical and electrophysiological data indicate that the AIS of cortical pyramidal neurons contains several different subtypes of ionic channels, including those conducting Na^+, K^+, and Ca^{2+} (Devaux et al., 2003, 2004; Inda et al., 2006; Pan et al., 2006; Vervaeke et al., 2006; Kole et al., 2007; Ogiwara et al., 2007; Lorincz and Nusser, 2008; Bender and Trussell, 2009; Hu et al., 2009). Calcium currents, like Na^+ and K^+ currents, are likely to contribute strongly to the electrophysiological properties of intracortical axons. Indeed, recent electrophysiological investigations of cartwheel cells in the cochlear nucleus, along with cortical pyramidal cells, suggest that Ca^{2+} currents may be prevalent in the axon initial segment and control the pattern of action potentials generated (Bender and Trussell, 2009). The ability of subthreshold depolarizations to alter baseline Ca^{2+} levels in axons suggests that calcium channels that are active below spike threshold may be prevalent in at least some portions of cortical axons and presynaptic terminals (Rusakov, 2006; Scott and Rusakov, 2006; Scott et al., 2008). This is particularly pertinent to the recent observation that somatic subthreshold depolarization can result in a significant increase in the strength of synaptic transmission between nearby neocortical pyramidal neurons, a process that is reduced or blocked by increases in the intracellular buffering of Ca^{2+} (Alle and Geiger, 2006; Shu et al., 2006b).

In the present study, we demonstrate that the AIS and proximal boutons exhibit prominent increases in Ca^{2+} concentration during subthreshold and suprathreshold membrane potential depolarization, and that much of this increase is mediated by P/Q and N Ca^{2+} channels. A key functional role for these calcium channels in the AIS is suggested as the block of P/Q and N channels results in a broadening of axonal action potentials, mediated at least in part through reduction of Ca^{2+}-dependent K^+ currents. Our results demonstrate that P/Q and N calcium channels play important roles in axonal action potential waveform, spike initiation, and the communication of subthreshold and suprathreshold membrane potentials to local synaptic boutons.

Received May 25, 2010; revised July 14, 2010; accepted July 19, 2010.
This work was funded by the National Institutes of Health and by the Kavli Institute for Neuroscience.
*Y.Y. and C.M. contributed equally to this work.
Correspondence should be addressed to David McCormick at the above address. E-mail: david.mccormick@yale.edu.
DOI:10.1523/JNEUROSCI.2651-10.2010
 0270-6474/10/3011858-12$15.00/0

Materials and Methods

Experiments were performed on slices of the male or female ferret (7- to 9-week-old) prefrontal cortex (anterior to the Sylvian fissure) maintained *in vitro*. Animals were anesthetized with sodium pentobarbital (150 mg/kg) and killed in accordance with the guidelines of the Yale University Institutional Animal Care and Use Committee. Slices (300 μm thick) were cut on a vibratome in an ice-cold solution containing the following (in mM): 2.5 KCl, 2 $MgSO_4$ 2 $CaCl_2$, 26, $NaHCO_3$, 1.2 NaH_2PO_4, 10 dextrose, and 215 sucrose, aerated with 95% O_2 and 5% CO_2 to a final pH of 7.4. Immediately after cutting, the slices were transferred to an incubation beaker filled with aerated (5% CO_2/95% O_2) normal artificial CSF (ACSF) containing the following (in mM): 126 NaCl, 2.5 KCl, 2 $MgSO_4$, 2 $CaCl_2$, 26 $NaHCO_3$, 1.25 NaH_2PO_4, and 10 dextrose (315 mOsm), pH 7.4. Slices were incubated at 35°C for 1 h before use. Then the slices were transferred to a submerged-style chamber at 36.5°C for recording with an aerated oxygenated recording ACSF solution that was the same as the incubation solution. Cortical neurons were visualized with an upright infrared differential interference contrast microscope (BX61WI; Olympus). Whole-cell recordings were achieved from the soma of layer 5 regular spiking neurons by using a Multiclamp 700B amplifier (Molecular Devices). Patch pipettes for somatic recording had an impedance of 3–6 MΩ (6–10 MΩ for AIS) and were filled with an intracellular solution that contained the following (in mM): 125 K-gluconate, 10 KCl, 4 ATP-Mg, 10 Na-phosphocreatine, 0.3 Na-GTP, 10 HEPES, and 0.2% biocytin, pH 7.2, with KOH (288 mOsm). The Ca^{2+} indicator Oregon Green 488 BAPTA-1 (0.05 or 0.1 mM; K_d of ~200 nM, green (Yasuda et al., 2004); preliminary experiments determined that 0.2 mM OGB1 blocked the ability of somatic depolarization to facilitate synaptic transmission between nearby cortical pyramidal neurons while 0.05 to 0.1 mM did not) (supplemental Fig. S1, available at www.jneurosci.org as supplemental material) as well as the morphological marker Alexa Fluor 594 (0.03–0.05 mM, red) were added to the pipette internal solution for two photon imaging. In some experiments, OGB1 was replaced with Fluo-5F (150 μM; K_d of ~1.4 μM at 21°C) (Woodruff et al., 2002; Yasuda et al., 2004). Experiments with Fluo-5F were typically performed at room temperature (21°C) so that the K_d of this dye was operating in the micromolar range. Results obtained at 35°C were similar to those obtained at 21°C, and therefore the results were combined for presentation (see supplemental Fig. S3, available at www.jneurosci.org as supplemental material). Calcium dyes were allowed to equilibrate for >20 min before line scans and xyt frame scans were performed. We present data as both the raw indicator fluorescence (F) as well as a ratio of the Alexa 594 signal (R) (F/R or $\Delta F/R$) to control for slow changes in dye concentration. For examining potential baseline changes in $[Ca^{2+}]_i$, we present the raw calcium indicator signal F as opposed to F/R since our data are presented as the average ratio of signal at −60 mV to that at −80 mV obtained from multiple interleaved trials. Thus, the R signals at −60 and −80 should, on average, be the same (and was observed to be so on measurement), and therefore would cancel out of the equation $(F_{-60}/R_{-60})/(F_{-80}/R_{-80})$, leaving simply F_{-60}/F_{-80}. Electrophysiological data were recorded at 30 kHz and filtered at 10 kHz using the Multiclamp 700B amplifier, and acquired using Spike-2 software (Cambridge Electronic Design). Action potentials were evoked via a somatic depolarization DC pulse (1–2 nA for 2 ms).

Two-photon excitation fluorescence imaging. Imaging of intracellular Ca^{2+} as well as cellular morphology was performed with a custom-made, two-photon laser-scanning microscope (Majewska et al., 2000) consisting of a modified Olympus Fluoview 300 Laser Scanning Confocal System and a MaiTai femtosecond pulsed (100 fs at 80 MHz) mode-locked Ti:Sapphire laser (Spectra-Physics; Newport). Laser intensity was adjusted to ~100 mW with a mirror before its entry into the modified confocal microscope. Fluorophores were excited in two-photon mode at 800 nm, and transfluorescence signals were captured through a 60×, 0.9 numerical aperture water-immersion objective (Olympus). The fluorescence signal was split into red and green channels using dichroic mirrors and bandpass filters (FV3-BA505-525; FV3-BA660IF) and detected by photomultiplier tubes (Hamamatsu). Fluorescence line scans were recorded at 800 Hz, and frame xyt scans (20 × 100 pixels) were recorded at 40 Hz (25 ms per frame) for capturing the calcium baseline and transient in different locations of recorded neurons.

Immunostaining. Postnatal ferrets (6 weeks) were anesthetized with sodium pentobarbital (30 mg/kg, i.p.) and perfused through the heart with freshly made 3% paraformaldehyde in ice-cooled PBS. The brains were removed and postfixed in the same fixative for 12 h. Coronal sections (40 μm) across the prefrontal cortex were made with a freezing microtome (Leica). The tissue sections were processed for floating immunolabeling as described below.

All sections were rinsed three times in 0.01 M PBS, pH 7.4, and then incubated in a blocking solution (3% BSA, 1% normal donkey serum, 0.3% Triton X-100 in PBS) at room temperature for 2 h. Sections were incubated overnight at 4°C with primary antibody against Cav2.1 (rabbit; 1:50; Santa Cruz Biotechnology) and Ankyrin G (goat; 1:200; Santa Cruz Biotechnology) or Cav2.2 (rabbit; 1:50; Alomone) and Ankyrin-G in 0.1% Triton X-100. After complete wash in 0.01 M PBS, these sections were incubated in Alexa-488-conjugated goat anti rabbit IgG and Alexa 543 goat anti mouse IgG in 0.1% Triton X-100 (1:200; Invitrogen). Sections were then mounted with Vectashield mounting media with 4′,6′-diamidino-2-phenylindole (DAPI; Vector Laboratories) and viewed on a laser-scanning confocal microscope (Zeiss LSM 510). All images were taken within the linear range of the photomultiplier. We processed three channels for every image separately but with the same procedures, one for calcium channel staining, the second for Ankyrin-G staining, and the third for DAPI. We did not observe significant interchannel cross talk. In the control group, slices were incubated without the use of primary antibodies. All controls revealed an absence of labeling.

Drug application. Local drug delivery to the axon/somatic region of recorded neurons was attained by brief (10–100 ms) puffing pulses of pressure adjusted to obtain small local application from the pipette (whole-cell recording electrode filled with the bath solution in which the toxin to be applied was dissolved). The drug delivery pipette was placed within ~10–50 μm of the axon initial segment. This application method allowed us to apply the drug rapidly and repeatedly without directly affecting ion channels in the apical dendrite or other distal portions of the neuron. It also reduced the quantity of toxin required, since our submerged slices required a high rate of perfusion (e.g., 2–3 ml/min).

Results

Calcium channels in the AIS and presynaptic terminals are sensitive to subthreshold and suprathreshold changes in membrane potential

We demonstrated previously that over a period of seconds the strength of synaptic transmission between locally connected cortical pyramidal cells is enhanced by somatic subthreshold membrane potential (V_m) depolarization through a Ca^{2+}-dependent mechanism (Shu et al., 2006a). To examine the effects of subthreshold V_m changes on resting and spike-triggered Ca^{2+} levels in the axon and presumed presynaptic boutons, we studied calcium concentration changes by using two-photon microscopy together with calcium fluorescence indicators. We performed whole-cell recordings from layer 5 pyramidal neurons in the ferret prefrontal cortex with pipettes containing either the fluorescence calcium indicator Oregon Green BAPTA 1 (50–100 μM) or Fluo-5F (150 μM) along with the non-calcium-binding indicator dye Alexa Red 594 (30 μM) for illustration of cellular morphology. Neurons were examined through either line or xyt scans.

After equilibration of the dyes within the neuron (>20 min; as evidenced by a lack of change in Alexa 594 fluorescence), the axon was localized as a nonspiny process emanating from the bottom of the soma that gave rise to beaded collaterals ~75–125 μm from the soma (Fig. 1*a*, see also Fig. 4*a*). Prefrontal layer 5 pyramidal neurons have an unmyelinated principal axon that extends toward the white mater for up to 300 μm in the slice (Shu et al., 2007b), with local axon collaterals that give rise to numerous presumed presynaptic boutons within layer 5 (identified as 1–3

μm swellings on axon collaterals occurring, on average, approximately every 10 μm) (Binzegger et al., 2004, 2005). We estimated the AIS, where action potentials are initiated in these neurons (Palmer and Stuart, 2006; Shu et al., 2007b), as the region of the axon that is 10 to 50 μm from the edge of the soma (Fig. 1*a*), and we considered the axon hillock to be the 10 μm conical-shaped axonal region connecting the AIS to the soma.

To examine the effect of changes in somatic membrane potential (which propagates down the axon) (Shu et al., 2006a) on axonal and presynaptic intracellular calcium concentration ($[Ca^{2+}]_i$) changes, we moved the somatic membrane potential of layer 5 pyramidal neurons (Fig. 1*a*) to approximately −80, −70, or −60 mV with current injection for periods of 10–20 s over multiple trials (Fig. 1*h*). At each membrane potential, we also triggered single action potentials with the somatic injection of a short-duration (2–4 ms) depolarizing current pulse once every 5 s. Since axonal baseline $[Ca^{2+}]_i$ levels were found to change over a period of 1 s or more to each membrane potential change, we plotted the Ca^{2+} levels just before or after an action potential initiated during the last 5 s of each period at a given membrane potential (Figs. 1, 2). The multiple trials were interleaved and averaged to control for slow changes in OGB1 or Fluo-5F response (e.g., because of bleaching or other changes in dye concentration or fluorescence).

Oregon Green BAPTA-1 was chosen for our investigations of baseline $[Ca^{2+}]_i$ because its high affinity for Ca^{2+} (K_d of ~200 nM at 35°C) (Yasuda et al., 2004) allowed us to detect small changes in resting $[Ca^{2+}]_i$ resulting from depolarization of the membrane potential. However, one consequence of this high affinity is that the examination of spike-evoked Ca^{2+} transients, which cause increases in general $[Ca^{2+}]_i$ throughout axonal processes that are in the hundreds of nanomolars or higher (Koester and Sakmann, 2000; Brenowitz and Regehr, 2007), may be impaired because of the sublinear fluorescence response of OGB1 to increases in free $[Ca^{2+}]_i$ at these high levels (Maravall et al., 2000; Yasuda et al., 2004; Higley and Sabatini, 2008). For this reason, to study spike-triggered changes, we performed experiments using the calcium indicator Fluo-5F (150 μM), which has a lower affinity for Ca^{2+} (K_d of ~1.4 μM at 21°C) (Woodruff et al., 2002; Yasuda et al., 2004). For OGB1, we used a concentration (50–100 μM) that did not disrupt the enhancement of EPSP amplitude between nearby pairs of layer 5 cortical pyramidal cells by subthreshold somatic depolarization of the presynaptic cell (supplemental Fig. S1*a*,*b*, available at www.jneurosci.org as supplemental material). Comparing the OGB1 and Fluo-5F responses to one, two, or a train of action potentials in the AIS and putative presynaptic boutons revealed that the ratio of F_{max}/F_{rest} was, on average, 2.25 for OGB1 (Scott et al., 2008) and 8.06 for Fluo-5F. Comparing the two calcium indicators in our system revealed that,

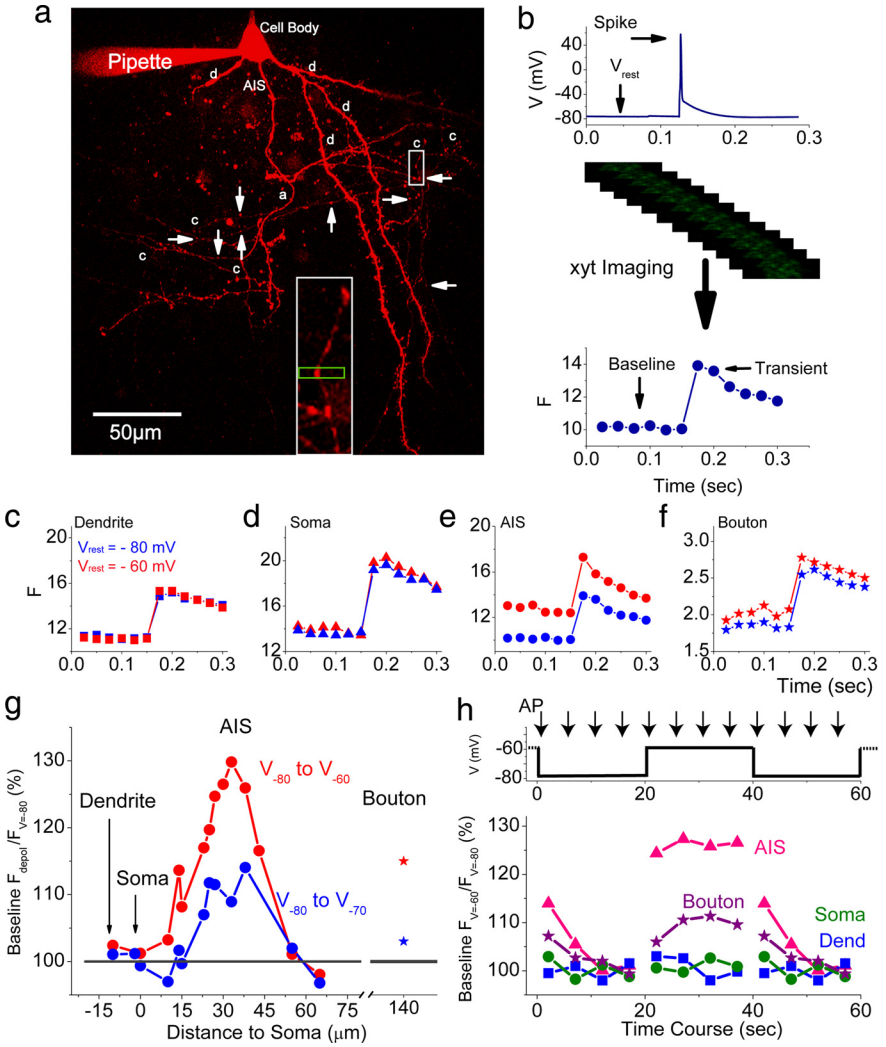

Figure 1. Depolarization increases resting $[Ca^{2+}]$ levels in the axon initial segment and proximal boutons. ***a***, Morphology of a recorded pyramidal cell showing the basal dendrites, main axon, and axon collaterals. The AIS and examples of axon collaterals (c), dendrites (d), and putative presynaptic boutons (arrows) are labeled. Inset, A typical x–y scan or line scan (which ever was chosen) around a putative presynaptic bouton. ***b***, The protocol involved initiation of an action potential through the intrasomatic injection of a brief (2 ms) current pulse once every 5 s while performing xyt two-photon imaging of a restricted region of the cell. The raw fluorescence value was then plotted as a function of time just before and after initiation of the single action potential. ***c–f***, Changes in the baseline membrane potential from −80 to −60 mV, induced through the intrasomatic injection of DC, result in no detectable change in the apical dendritic (30 μm apart from cell body) (***c***) or somatic (***d***) baseline Ca^{2+} levels, but a significant upward shift in Ca^{2+} concentrations in the axon initial segment (30 μm apart from cell body) (***e***) and a small upward shift in a proximal putative presynaptic bouton (140 μm apart from cell body) (***f***). ***g***, Plot of the average ratio of Ca^{2+} indicator dye (OGB1) fluorescence at −60 mV to that at −80 mV and from −70 to −80 mV as a function of distance from the soma. Note that there is a significant increase at the axon initial segment, followed by a drop off to no change in the distal axon. Putative presynaptic boutons, however, do exhibit a significant increase in baseline Ca^{2+} concentration with depolarization (stars). For this figure and others, the ratio of average fluorescences (e.g., F_{-60}/F_{-80}) was plotted instead of $(F_{-60}/R_{-60})/(F_{-80}/R_{-80})$ since average R_{-60} and R_{-80} values were found to be identical (see Materials and Methods). ***h***, Time course of changes in Ca^{2+} in the AIS and presynaptic boutons. A change in membrane potential between −60 and −80 mV was induced with somatic current injection every 20 s over multiple trials. The plot represents the average of the response either to a step from −80 to −60 or vice versa. Thus, the data before and after the depolarizing step to −60 are identical and represent the average response to a hyperpolarizing step from −60 to −80 mV. Ca^{2+} levels in the AIS and presynaptic boutons change slowly over several seconds during these step changes in membrane potential. Action potentials were initiated every 5 s as indicated by the arrows (AP). Error bars in all figures indicate SEM.

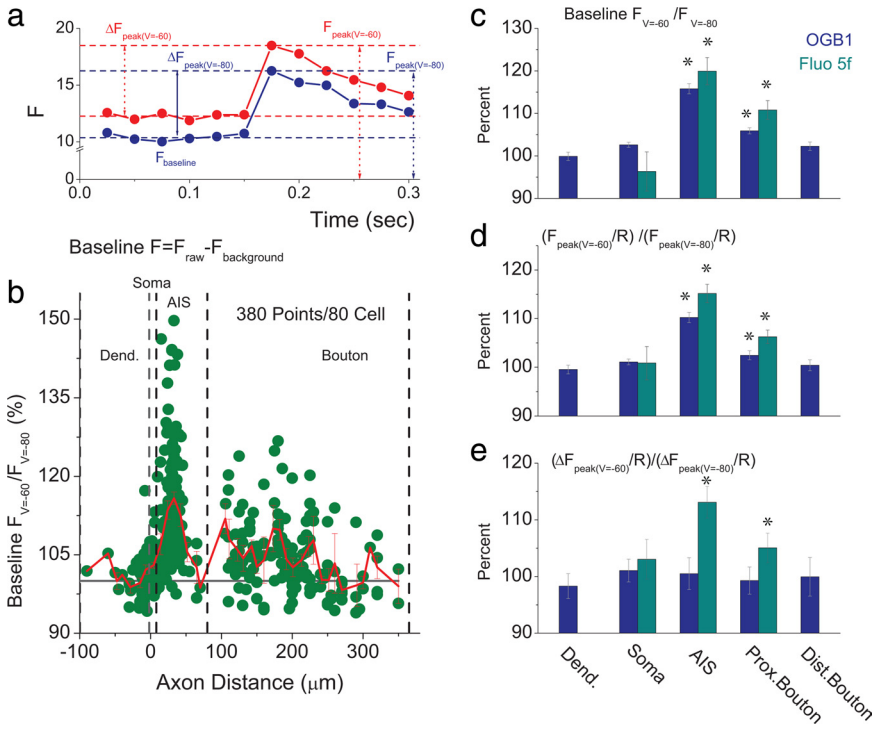

Figure 2. Baseline and spike-triggered Ca^{2+} levels are enhanced by depolarization. ***a***, Raw examples illustrating the measures taken, including baseline F, F_{peak}, which is the absolute value of the peak amplitude of F after a spike, and ΔF_{peak}, which is the difference between F_{peak} and $F_{baseline}$. All values are after substraction of background fluorescence. Pipette contained OGB1. ***b***, Plot of individual measures of percentage change in baseline Ca^{2+} indicator dye fluorescence with depolarization from approximately −80 to −60 mV versus distance along the axon (or dendrite) from the soma. Note the large changes occurring in the axon initial segment, and the smaller percentage increases occurring in putative presynaptic boutons of axon collaterals. Individual measures ($n = 380$ from 80 neurons) are shown. The thick solid trace represents the average response, whereas the thin vertical lines illustrate ±SEM. Nearly all points distal to the AIS are measurements from putative presynaptic boutons (as identified by swellings spaced a few micrometers apart). The pipette contained OGB1. ***c***, Averaged effects of depolarization on baseline and spike-triggered rises in OGB1 and Fluo-5F fluorescence with somatic depolarization. Top, Tonic somatic depolarization causes an increase in baseline fluorescence in both the AIS and proximal (<200 μm) boutons for both OGB1 and Fluo-5F recordings. ***d***, Similarly, examining the peak amplitude of spike-triggered fluorescence change with somatic depolarization (plotted as F_{peak}/R) also revealed significant increases in the AIS and proximal boutons for both of these indicator dyes. ***e***, The spike-triggered change in fluorescence ($\Delta F_{peak} = F_{peak} - F_{baseline}$) was significantly enhanced by somatic depolarization in the AIS and proximal boutons for the indicator dye Fluo-5F, but not for OGB1. The response of both dyes were measured as $\Delta F/R$. Error bars represent SEM. Asterisks indicate significant effects ($p < 0.05$).

although neither dye reached saturation with single action potentials, each action potential evoked a much smaller change in fluorescence (ΔF/R) in the AIS for OGB1 than for Fluo-5F (supplemental Fig. S2, available at www.jneurosci.org as supplemental material).

We examined three different parameters of calcium indicator response: fluorescence baseline ($F_{baseline}$), peak spike-triggered fluorescence (F_{peak})/R (where R is the fluorescence signal intensity in the Alexa 594 channel, which is calcium insensitive), and $\Delta F/R$ (Yasuda et al., 2004) (commonly referred to as $\Delta G/R$) (Figs. 1, 2). For examination of the changes in prespike baseline [Ca^{2+}] induced by subthreshold depolarization, we plot the ratio of raw prespike OGB1 fluorescence brightness at the depolarized membrane potential to that at the hyperpolarized or resting membrane potential (Fig. 1*g*).

For each location in the example cell (Fig. 1*c–f*), a set of 12 frames (x–y scans) was captured at 40 Hz (25 ms/frame) to quantify calcium dynamics: five (or six) frames before (125–150 ms) and six (or seven) after (150–175 ms) an action potential (Fig. 1*b*). The baseline fluorescence was taken as the average OGB1 signal (five- or six-frame average intensity, 0 to 125 ms) before action potential initiation. The transient fluorescence represents the response of OGB1 to the transient increase in $[Ca^{2+}]_i$ that occurs throughout the cellular process under investigation (e.g., AIS or presynaptic bouton) in response to a single action potential (averaged over 0 to 50–75 ms after the spike). It should be noted that this general increase in $[Ca^{2+}]_i$ within the process under examination in response to an action potential is less than that occurring in local domains close to the Ca^{2+} channels activated by the spike and that its time course is slowed considerably by the properties of the dye (Yasuda et al., 2004). The frequency of our data collection also limits our ability to observe fast time constants.

The baseline OGB1 fluorescence did not change significantly in the apical dendrite (10–40 μm away from cell body) (Fig. 1*c*) and cell body (Fig. 1*d*) when the soma was depolarized from −80 to −60 mV for a period of 20 s, indicating that this manipulation did not affect baseline$[Ca^{2+}]_i$ in these portions of the neuron. However the same depolarization resulted in a large increase (>20%) of baseline OGB1 fluorescence in the AIS (30 μm away from cell body) (Fig. 1*e*,*g*; supplemental Fig. S1*c–e*, available at www.jneurosci.org as supplemental material). A smaller but detectable increase (~5–15%) in OGB1 fluorescence baseline was observed in proximal presynaptic boutons (within 250 μm of the cell body) (Fig. 1*f*,*g*). Examining the effect of changes in membrane potential along several locations from the basal portions of the apical dendrite through the soma and down the axon revealed distance-dependent effects when the soma was depolarized from −80 to either −70 or −60 mV for 20 s (Fig. 1*g*). These subthreshold depolarizations resulted in marked increases in resting calcium levels (represented as a ratio $F_{depol}/F_{v=-80}$) in the AIS, with a maximum ~30 μm from the soma. This effect was not detectable at axonal distances of ~60 μm or greater from the soma, except at nearby putative presynaptic boutons (Fig. 1*g*). Examining the time course of this effect revealed that the changes in Ca^{2+} levels in the AIS and presynaptic boutons display a prominent slow component in this cell, increasing and decreasing slowly over 1 s or longer (Figs. 1*h*, 3). In contrast to the localized effect of subthreshold membrane potential on Ca^{2+} levels in the AIS and presynaptic boutons, action potentials caused marked increases in Ca^{2+} levels in all cellular regions measured (Fig. 1*c–f*).

Ensemble statistics of baseline and transient calcium dynamics

The effects of change in somatic membrane potential on baseline and evoked Ca^{2+} levels were examined in a total of 380 locations from 80 different layer 5 pyramidal neurons with OGB1 (Fig. 2). As observed in the single neuron of Figure 1, the group data confirmed that subthreshold depolarization of the soma for 20 s has a strong effect on baseline Ca^{2+} levels in the AIS, peaking at

25–40 μm from the soma (mean, 115.8 ± 1.2%; $n = 92$; $p < 0.001$) (Fig. 2*b*,*c*). Somatic depolarization-induced increases in baseline Ca^{2+} levels were also observed in putative presynaptic boutons at distances of between 100 and 225 μm from the soma (Fig. 2*b*), where a depolarization of the soma from −80 to −60 mV resulted in an increase in OGB1 fluorescence, typically between 3 and 8%, but sometimes as high as 25% (mean, 5.9 ± 0.3%; $n = 131$; $p < 0.001$). At distances between 225 and 350 μm (the longest distance tested), this effect was not statistically significant (mean, 1 ± 0.9%; $n = 44$; $p > 0.05$). In the cell body and proximal locations (<40 μm from soma) of the basal and apical dendrites, no subthreshold depolarization-sensitive calcium response was clearly observed (somatic change in OGB1 fluorescence, 2.6 ± 0.6%; $n = 15$; $p > 0.05$; dendritic change, −0.1 ± 1%; $n = 37$; $p > 0.05$).

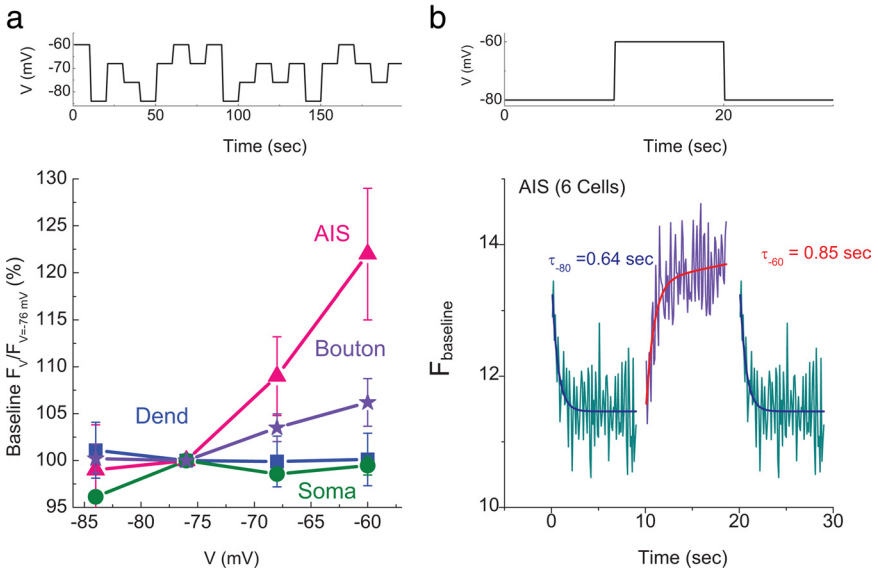

Figure 3. Baseline changes in calcium are voltage and time dependent. ***a***, Protocol for changing the membrane potential of a neuron to examine the change in baseline Ca^{2+} at different membrane potentials. The cell was randomly moved to each membrane potential for 10 s, and Ca^{2+} indicator fluorescence (OGB1) was measured near the end of each depolarizing step. Bottom, Plot of percentage change in Ca^{2+} indicator dye fluorescence versus membrane potential for the different compartments measured demonstrates that in both the AIS and presynaptic boutons, baseline Ca^{2+} levels gradually increase with depolarization above approximately −75 mV. ***b***, Narrow xyt scan (200 Hz) of the AIS during steps in membrane potentials between −80 and −60 mV revealed baseline Ca^{2+} to change with a slow time constant of 0.64 s during depolarization and 0.85 s during hyperpolarization. Error bars represent SEM.

We examined the effects of tonic membrane potential depolarization on the changes in OGB1 and Fluo-5F fluorescence evoked by single action potentials (Fig. 2*a*) (as measured over the 25–75 ms after a spike). Depolarization of the membrane potential from −80 to −60 mV resulted in a significant increase in the absolute peak amplitude obtained by spike-evoked OGB1 and Fluo-5F fluorescence (F_{peak}/R) in both the AIS and proximal presynaptic boutons (Fig. 2*d*). This result indicates that tonic depolarization increases the peak levels of $[Ca^{2+}]_i$ occurring in these structures in response to the generation of an action potential. Measurement of the spike-evoked change in fluorescence normalized to the Alexa 594 fluorescent signal ($\Delta F/R = (F_{peak} - F_{baseline})/R$) revealed that depolarization of the soma from −80 to −60 mV resulted in no significant change in spike-evoked $\Delta F/R$ for OGB1 in both the AIS (100.5 ± 2.8%; $n = 92$) and proximal presynaptic boutons (99.3 ± 2.4%; $n = 131$). However, when we reexamined this issue with the lower-affinity calcium indicator dye Fluo-5F, which yields a much larger fluorescent signal per action potential (Fig. 2*e*; supplemental Fig. S2, available at www.jneurosci.org as supplemental material), we found that depolarization of the soma from −80 to −60 mV resulted in a significant increase in spike-evoked $\Delta F/R$ in the AIS (13.1 ± 3.2%; $n = 50$) and proximal presynaptic boutons (5.1 ± 2.6%; $n = 38$), but not the soma (3.0 ± 3.5%; $n = 8$). Together, these results indicates that depolarization of the soma results in an increase in spike-evoked $[Ca^{2+}]_i$ transients in both the AIS and nearby presynaptic boutons.

To study in detail the dependence of baseline calcium levels on somatic membrane potential, the cell body membrane potential was randomly changed to four different levels from approximately −85 to −60 mV for 10 s each (Fig. 3*a*). For both the AIS and presynaptic boutons, depolarization of the soma to levels above approximately −75 mV resulted in detectable increases in baseline Ca^{2+} levels (as measured at the end of each 10 s period with OGB1) in the AIS and proximal presynaptic boutons, and these increases grew proportionally larger with increased depolarization (Fig. 3*a*).

We examined the time course of changes in baseline Ca^{2+} levels for group data using the two-level step protocol (Fig. 3*b*) while imaging OGB1 fluorescence with a narrow xyt scan at 200 Hz. Average baseline Ca^{2+} levels in the AIS (~30–40 μm from cell body) exhibited a slow increase (rising $\tau = 0.64 \pm 0.19$ s; $n = 5$ cells) during depolarization and a slow decrease (falling $\tau = 0.85 \pm 0.34$ s; $n = 5$) during hyperpolarization.

The effect of depolarization on resting Ca^{2+} levels requires transmembrane Ca^{2+} influx

To investigate whether the subthreshold somatic depolarization induced calcium response in AIS and presynaptic boutons arises from membrane-potential-gated calcium channels or internal calcium stores, we blocked transmembrane Ca^{2+} influx by replacing Ca^{2+} with Mn^{2+} in the extracellular bathing solution. This manipulation nearly abolished the subthreshold depolarization-induced calcium response and action-potential-evoked calcium transient ($\Delta F/R$) in the AIS and presynaptic boutons (Fig. 4) (88 ± 4%, 92 ± 3% and 93 ± 3%, 89 ± 2% block of baseline and transient Ca^{2+} response in AIS and boutons, respectively; $n = 67$ observations in 11 cells; OGB1). Returning $[Ca^{2+}]_o$ to normal and removing Mn^{2+} from the bathing solution reversed this block. In additional experiments, including 10 mM Ca^{2+} chelator EGTA in the micropipette reduced the depolarization-induced increase in baseline response by 92 ± 2% in the AIS and by 98 ± 2% in presynaptic boutons (Fig. 4*d*,*e*). Similarly, the spike-triggered increase in Ca^{2+} indicator fluorescence was reduced by 86 ± 5% (AIS) and 88 ± 3% (boutons) by inclusion of 10 mM EGTA in the recording pipette ($n = 58$ observations in 10 cells) (Fig. 4*d*,*e*).

These results indicate that the ability of subthreshold somatic depolarization to increase baseline Ca^{2+} level, as well the spike-triggered increases in average internal Ca^{2+} concentration, depend on the transmembrane flow of Ca^{2+}, suggesting that they are mediated by the activation of voltage-sensitive Ca^{2+} channels.

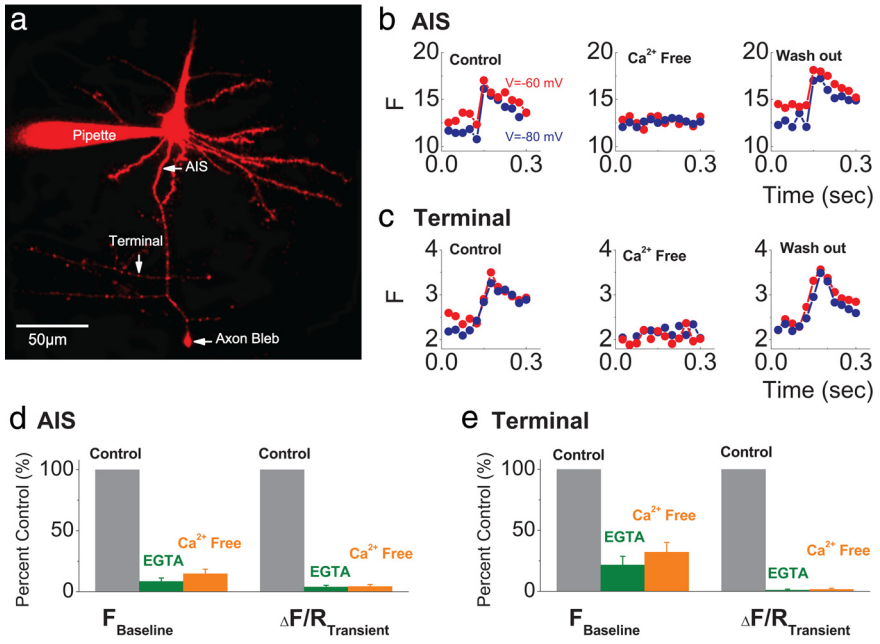

Figure 4. The effects of depolarization on Ca^{2+} concentrations are antagonized by buffering internal Ca^{2+} or blocking transmembrane Ca^{2+} entry. ***a***, Morphology of the studied neuron. ***b***, ***c***, Reduction of $[Ca^{2+}]_o$ to 0 mM (and replacement with Mn^{2+}) resulted in a block of the action potential-induced transient increase in Ca^{2+} in the AIS, as well as the ability of somatic depolarization to influence basal Ca^{2+} levels. This effect was reversible with return of $[Ca^{2+}]_o$ to normal (washout). ***d***, Including 10 mM EGTA or removal of external Ca^{2+} nearly completely blocked the effect of changes in membrane potential on baseline Ca^{2+} levels in the AIS and presynaptic boutons. ***e***, These manipulations also blocked the spike-evoked increase in Ca^{2+} concentrations in the AIS and presynaptic boutons. Error bars represent SEM.

P/Q- and N-type Ca^{2+} channels mediate the baseline and spike-triggered Ca^{2+} responses in the AIS and presynaptic boutons

The identification of the Ca^{2+} channels that mediate the effects observed here was determined through pharmacological manipulations. Bath application of 50–200 μM $NiCl_2$ blocked the ability of subthreshold depolarization to increase baseline Ca^{2+} levels (supplemental Fig. S4, available at www.jneurosci.org as supplemental material) ($n = 74$ observations in nine cells). Although Ni^{2+} has been reported to be a selective blocker of T-type Ca^{2+} channels, this divalent cation can also block Ca^{2+} currents of other varieties (Magee and Johnston, 1995; Zamponi et al., 1996), and therefore is not specific. Indeed, we did not find any clear blocking effect of three different antagonists of low-threshold-activated calcium channels: NNC 55-0396 [(1*S*,2*S*)-2-(2-(*N*-[(3-benzimidazol-2-yl)propyl]-*N*-methylamino)ethyl)-6-fluoro-1,2,3,4-tetrahydro-1-isopropyl-2-naphtyl cyclopropanecarboxylate dihydrochloride] (Huang et al., 2004) (10–100 μM; $n = 26$ observations in five cells) (supplemental Fig. S5, available at www.jneurosci.org as supplemental material), mibefradil dihydrochloride (Martin et al., 2000) (3–30 μM; $n = 76$ observations in seven cells; mibefradil actually significantly enhanced the Ca^{2+} baseline response) (supplemental Fig. S6, available at www.jneurosci.org as supplemental material), and fluoxetine (Traboulsie et al., 2006) (30–50 μM; $n = 18$ observations in two cells) (supplemental Fig. S7, available at www.jneurosci.org as supplemental material). These results indicate that T-type Ca^{2+} channels are unlikely to mediate the effects induced by somatic membrane depolarization on baseline AIS calcium levels.

Application of $C_{192}H_{274}N_{52}O_{60}S_7$ (SNX482) (0.5 μM; $n = 30$ observations in five cells), which is reported to be a selective antagonist for Cav2.3 (R-type) channels, resulted in a 12 ± 8.6% decrease in the effect of change in baseline membrane potential on transient Ca^{2+} levels in the AIS (supplemental Fig. S8, available at www.jneurosci.org as supplemental material). Although this result suggests that R-type calcium channels may make a small contribution to this response, it is also possible that this reduction resulted from an effect of SNX482 on P/Q calcium channels (Arroyo et al., 2003). Here we concentrate on the role of N and P/Q channels in the AIS and presynaptic boutons, since applications of specific antagonists to these channels blocked nearly all of the effects we observed (see Fig. 5).

Bath applications of either the P/Q channel (Cav2.1) antagonists ω-agatoxin TK or ω-agatoxin IVA (0.5 μM) or the N channel (Cav2.2) antagonist ω-conotoxin GVIA (2 μM) (Currie and Fox, 1997) nearly abolished the ability of subthreshold membrane potential changes to affect baseline Ca^{2+} levels in the AIS and proximal presynaptic boutons (Fig. 5). Similarly, these antagonists also decreased significantly the Ca^{2+} transients triggered by single action potentials in both the AIS and presynaptic boutons (Fig. 5). Group statistics revealed that in the AIS, ω-agatoxin blocked 73.7 ± 3.9% ($n = 40$ observations in 10 cells) of the baseline response to depolarization (Figs. 5*c*). Similarly, conotoxin blocked 85.7 ± 5.% of the subthreshold AIS response, and when applied simultaneously, these drugs blocked 89.5 ± 3.0% ($n = 107$ observations in 17 cells) of the baseline $[Ca^{2+}]_i$ response to depolarization (Fig. 5). Likewise, these antagonists also blocked the baseline change in Ca^{2+} at presynaptic terminals with subthreshold depolarization: ω-agatoxin blocked 93.5 ± 1.2% ($n = 136$ observations in 21 cells), ω-conotoxin blocked 97.2 ± 1.1% ($n = 107$ observations in 17 cells), and both toxins applied together blocked 98.5 ± 1.1% ($n = 74$ observations in 16 cells) (Fig. 5).

Examining the effect of these two antagonists on the spike-dependent Ca^{2+} transient in the AIS revealed that ω-agatoxin blocked 53 ± 6.8% (same *n* values as above for effects on baseline Ca^{2+} levels), ω-conotoxin blocked 52 ± 7.9%, and both toxins applied together blocked 60 ± 5.2% (Fig. 5). In presynaptic terminals, agatoxin and conotoxin also exhibited strong effects. Agatoxin application blocked the spike-triggered increase in Ca^{2+} by 70 ± 7.8%, whereas conotoxin blocked 56 ± 9.6%, and application of both toxins blocked 83 ± 6.8% of the original response (Fig. 5).

Interestingly, we noticed that these results varied from cell to cell. Whereas the application of both toxins together always resulted in a large reduction in the baseline and spike-triggered Ca^{2+} responses, the application of agatoxin or conotoxin alone had variable effects (Fig. 5). These data suggest N and P/Q channels vary in the strength of their contributions to baseline and spike-triggered Ca^{2+} transients in the AIS, with some neurons exhibiting a strong dependence on N channels and others being more dependent on P/Q Ca^{2+} currents (Fig. 5).

Together, the individual effects of agatoxin and conotoxin add to >100% block. Although the origin of this nonlinearity is unknown, one relevant factor is the slow rundown in the Ca^{2+} or OGB1 response over the 2–3 h required to perform these exper-

iments, as noted previously (Koester and Sakmann, 2000). In cells in which agatoxin or conotoxin were not applied, we observed a rundown in OGB1 response to action potentials in the range of 10–30% over this time period. Despite this limitation, our results indicate that the subthreshold depolarization-sensitive calcium currents may be mainly of the P/Q and N variety in the AIS and presynaptic boutons.

Immunocytochemical localization of P/Q and N channels in the axon initial segment

Our pharmacological and two-photon imaging studies suggest that P/Q- and N-type Ca^{2+} channels make a significant and important contribution to transmembrane Ca^{2+} signals in the axon initial segment. We examined this further by performing immunocytochemical staining for P/Q- and N-type Ca^{2+} channels in the AIS of presumed pyramidal cells in prefrontal cortex of 6- to 9-week-old ferrets by using selective Cav2.1 and Cav2.2 antibodies (see Materials and Methods) (Lopez et al., 1999). Costaining for the Na^+ channel-associated protein ankyrin-G was used to localize the AIS (Inda et al., 2006), whereas costaining for DAPI revealed the location of cellular nuclei (Fig. 6). We focused our examination on layer 5, which also had the clearest and most prominent labeling of apparent axon initial segments by our antibodies.

Immunocytochemical localization of ankyrin-G revealed the presence of lines of staining beneath immunonegative cell bodies, the nuclei of which were stained with DAPI, demonstrating the presence of the AIS of cortical neurons (Fig. 6). Costaining for Ca2.1 (P/Q) channels and ankyrin-G revealed nearly complete overlap for the AIS (Fig. 6*a*), indicating that this axonal region may contain a high density of P/Q channels. Immunocytochemical localization of Cav2.2 (N-type) channels (Fig. 6*b*) also revealed extensive overlap with ankyrin-G staining at the AIS segment, demonstrating that this neuronal compartment also contains these Ca^{2+} channel subunits. A high degree of staining in the background neuropil, including cell bodies and putative dendritic structures, suggests that this Ca^{2+} channel subunit may have a widespread distribution.

Although these immunostaining results do not yield a precise quantitative estimation of calcium channel distributions in AIS compared with the cell body, the results in Figure 6 provide clear evidence that the AIS contains both P/Q- and N-type calcium channels in neurons of the ferret prefrontal cortex.

Functional role of P/Q- and N-type channels in AIS

Our immunohistochemical, calcium imagining, and pharmacological results suggest an important role for P/Q- and N-type calcium channels in AIS physiology. Next, we examined the functional role of P/Q- and N-type Ca^{2+} channels in layer 5 pyramidal neurons through local coapplication of ω-agatoxin and ω-conotoxin while evaluating the excitability properties of the AIS.

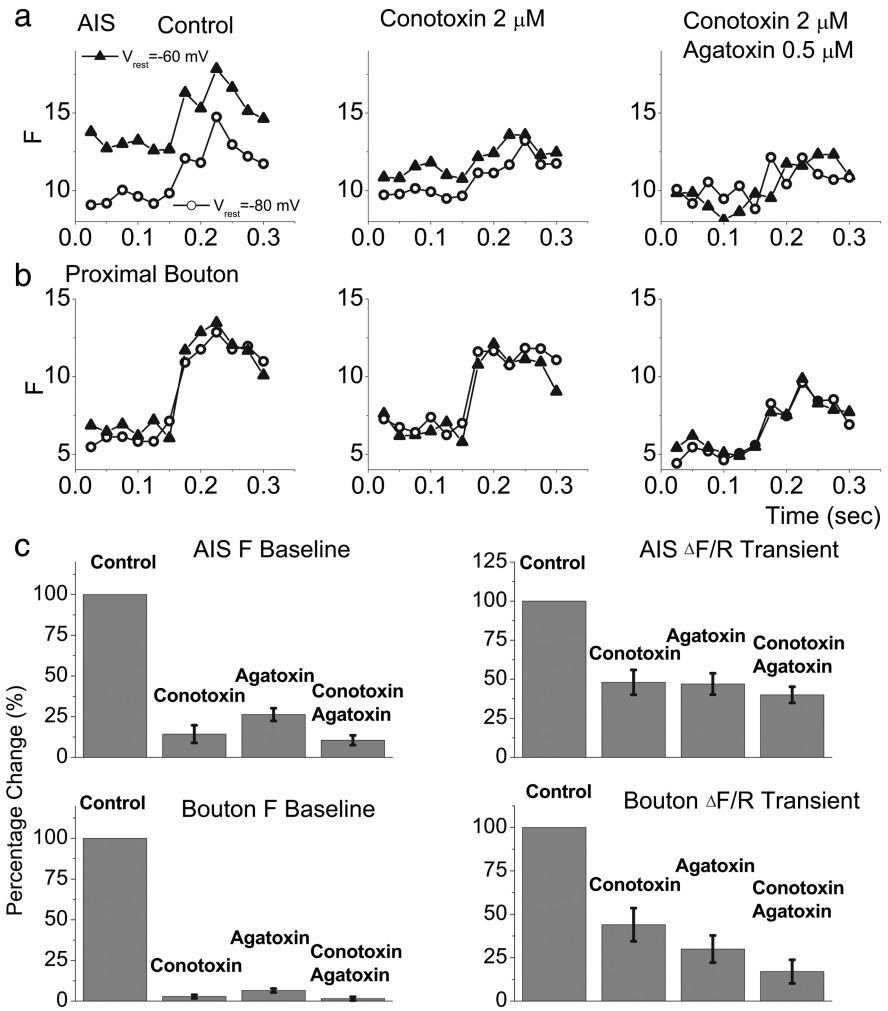

Figure 5. Subthreshold depolarization-induced and spike-triggered increases in intracellular Ca^{2+} levels depend on N and P/Q Ca^{2+} channels. ***a***, Bath application of the N-channel blocker ω-conotoxin GVIA (2 μM) results in a block of the subthreshold depolarization induced increase in baseline Ca^{2+} concentration in the AIS as well as a significant reduction in spike-triggered changes in Ca^{2+}. Addition of the P/Q channel blocker ω-agatoxin IVA (0.5 μM) results in an additional decrease in the spike-triggered Ca^{2+} response. ***b***, Similar results are observed in presynaptic boutons. ***c***, Group data demonstrating that application of either ω-conotoxin GVIA or ω-agatoxin IVA results in a large decrease in subthreshold depolarization induced or spike-triggered induced increase in AIS and bouton Ca^{2+} levels. Application of ω-conotoxin GVIA and ω-agatoxin IVA together has a slightly greater effect than either antagonist alone. Error bars represent SEM.

We obtained patch-clamp whole-cell recordings from either the soma or axon (on or near the AIS, between 30 and 100 μm from the soma), or both simultaneously (Shu et al., 2006a, 2007b). Depolarization of layer 5 pyramidal neurons with a 1 s depolarizing current pulse injected either into the soma or the AIS resulted in a train of action potentials, with the duration of each action potential increasing during the train (Fig. 7*b*). This duration increase expressed itself as a slowing of, and the appearance of a depolarizing bump on, the repolarizing phase of the action potential, in both the axon (Fig. 7*b*) ($n = 14$) and soma (Fig. 8*a*) ($n = 17$). There was a particularly large increase in duration between the first and subsequent action potentials (Fig. 7*b*). The effects of local puffer application of agatoxin (50 μM in micropipette) and conotoxin (15 μM in micropipette) were examined while recording either from the AIS ($n = 14$), the soma ($n = 17$), or both simultaneously ($n = 3$). Local block of N and P/Q channels in the AIS/somatic region resulted in a small but

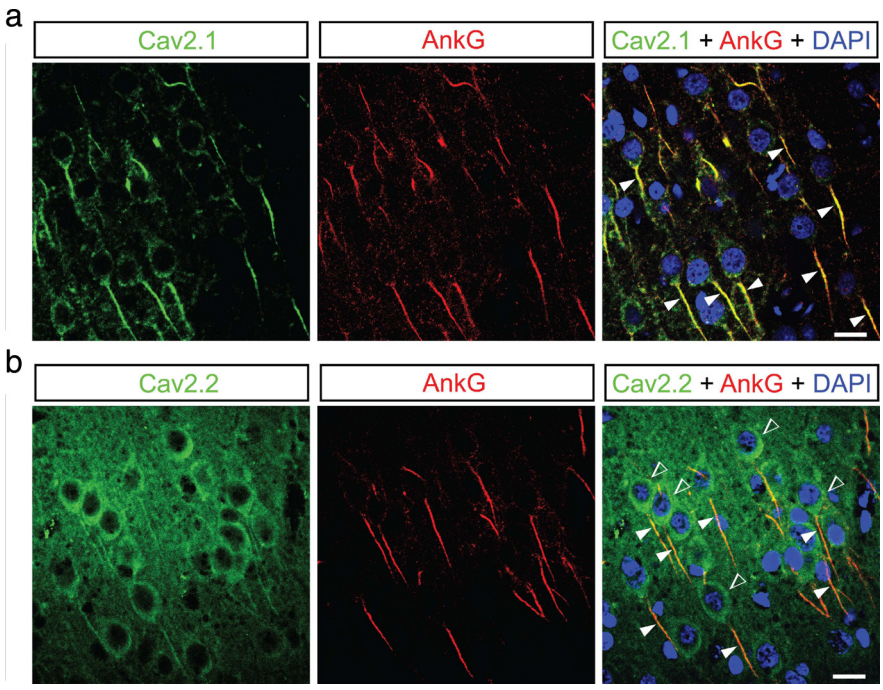

Figure 6. Axon initial segment contains both Cav2.1 (α1A; P/Q-type) and Cav2.2 (α1B; N-type) subunits. ***a***, Immunocytochemical localization of Cav2.1, ankyrin-G (AnkG), which is prevalent in axon initial segments of cortical pyramidal cells, and DAPI, which marks nuclei in the ferret prefrontal cortex. The overlap of all three stains is shown on the right. Note that both Cav2.1 and ankyrin-G are prevalent in cortical axon initial segments, as revealed by ankyrin-G staining. ***b***, Immunocytochemical localization of Cav2.2 and ankyrin-G demonstrating that the AIS also contains this subtype of Ca^{2+} channel protein. Cav2.2 was also prevalent in the somata and neuropil of the neocortex, causing a higher background than seen with antibodies to Cav2.1 (***a***). Solid arrowheads, AIS with calcium channels staining in cells; open arrowheads, cell body. Scale bar, 15 μm.

statistically significant increase in duration of the action potential in the AIS (8 ± 3%; $n = 14$; measured at half-height) (Fig. 7*b*,*c*). This increase in duration was most prominent during the later parts of spike repolarization as well as during the later action potentials in the spike train (Fig. 7*b*). Interestingly, the local combined application of agatoxin and conotoxin resulted in a small decrease in spike duration in the soma (−8 ± 2%; $n = 17$). Simultaneous recording of action potentials from the soma and AIS revealed that local application of agatoxin and conotoxin resulted in a lengthening in action potential duration in the AIS, whereas the same action potentials were shortened in duration in the soma (data not shown) ($n = 3$ dual recordings).

In addition to increasing the duration of action potentials in the AIS, the local application of combined agatoxin and conotoxin resulted in an increase in neuronal excitability as expressed by an increase in the slope of the frequency versus current plot (Fig. 7*d*). Each axon or somatic recording was subjected to three different current pulse amplitudes. In control conditions, the smallest amplitude current pulse caused the axon/soma to discharge at an average frequency of 3.3 ± 0.7 Hz, whereas the middle amplitude caused discharge at 8.5 ± 1.3 Hz, and the largest drove the process at 14.7 ± 2.5 Hz. Plotting the change in action potential frequency after application of agatoxin/conotoxin versus control for each of three current pulse amplitudes used (Fig. 7*d*; current pulses 1, 2, and 3) revealed a consistent increase in discharge frequency for the middle and larger amplitude pulses, indicating an increase in excitability. This increase in excitability was not associated with any significant change in apparent input resistance (R_m), action potential threshold, or baseline membrane potential (Fig. 7*e*).

We hypothesized that the increase in duration of the AIS action potential in response to block of P/Q and N channels may have resulted from reduced activation of a Ca^{2+}-activated K^+ current, such as that mediated by Big Potassium (BK) channels [ion channels characterized by their large conductances of potassium ions through cell membranes. These channels are activated by changes in membrane potential and/or by increases in concentration of intracellular calcium Ca^{2+} (Galvez et al., 1990)]. To test this hypothesis, we examined the effects of local application of iberiotoxin (IBTx), a potent antagonist of BK channels (Galvez et al., 1990), on AIS and somatic spike duration. Local application of IBTx (10 μM in micropipette) resulted in a broadening of action potentials in the AIS (by 17 ± 4%; $n = 13$), indicating that these Ca^{2+}-activated K^+ channels make a significant contribution to spike repolarization in this cellular region (Fig. 8). As with the local application of agatoxin/conotoxin, this broadening was prominent during the later portions of the repolarizing phase of the action potential (Fig. 8). The action potential broadening effect of IBTx was significantly smaller in the soma (7 ± 2%; $n = 10$) (Fig. 8). The application of iberiotoxin did not alter baseline membrane potential or the frequency of action potential discharge to the injection of current pulses (Fig. 8*c*). This result supports the hypothesis that the BK class of Ca^{2+}-activated K^+ channels plays an important role in repolarization of action potentials in the AIS, with a less prominent role in the soma, of layer 5 cortical pyramidal neurons.

After the block of BK channels and broadening of action potentials in the AIS with iberiotoxin, we applied agatoxin and conotoxin locally to the AIS. Whereas in normal solution the block of P/Q and N channels normally caused a small increase in action potential duration in the AIS, after the reduction of Ca^{2+}-activated K^+ currents, application of agatoxin and conotoxin resulted in a small but significant decrease (−7 ± 1%; $n = 7$) in the duration of the prolonged action potentials in the AIS (data not shown). This result suggests that at least part of the prolonged AIS action potentials, after block of BK channels, are mediated by Ca^{2+} entry through P/Q and N channels.

Discussion

Our results demonstrate that the axon initial segment and intracortical presynaptic boutons of layer 5 pyramidal cells contain N and P/Q Ca^{2+} channels that are activated by subthreshold and suprathreshold depolarizations, contributing significantly to the physiological and functional properties of these neuronal processes. Subthreshold depolarization of 10–20 mV resulted in an increase in baseline and spike-triggered Ca^{2+} levels in the AIS and nearby presynaptic boutons. We hypothesize that this increase in baseline spike-triggered Ca^{2+} levels may contribute to a previously observed ability of subthreshold depolarization to facilitate synaptic transmission between nearby pyramidal neurons (Shu et al., 2006a). The Ca^{2+} channels of the AIS regulate neu-

ronal excitability, in part by activating a Ca^{2+}-activated K^+ current that is partially responsible for spike repolarization as well as by controlling the relationship between local current flow and neuronal firing rate. These results demonstrate that P/Q and N Ca^{2+} channels make important, previously unknown contributions to the properties of the axon initial segment and presynaptic boutons.

Implications of subthreshold changes in axonal Ca^{2+}

We demonstrated previously that subthreshold depolarization of the soma of a layer 5 pyramidal neuron results in an average 30% enhancement of excitatory synaptic transmission between that neuron and its neighboring pyramidal cells (Shu et al., 2006a). Similarly, depolarization of the dendrites and cell bodies of granule neurons in the hippocampus can result in a significant increase in synaptic transmission at mossy fiber boutons onto CA3 pyramidal cells (Alle and Geiger, 2006). Subthreshold depolarization of presynaptic terminals in the calyx of Held results in significant increases in baseline $[Ca^{2+}]_i$ as well as large increases in synaptic transmission (Awatramani et al., 2005). The time constant of this facilitation of synaptic transmission as well as the increase in baseline $[Ca^{2+}]_i$ (which appears to be mediated at least in part by the activation of P/Q channels) was ~1–3 s. Buffering internal Ca^{2+} levels with the presynaptic injection of EGTA, both in the calyx of Held and in the neocortex, blocked the ability of subthreshold depolarization to facilitate synaptic transmission, suggesting that these two effects may be casually related (Awatramani et al., 2005; Shu et al., 2006a). However, intracellular buffering of Ca^{2+} did not completely block depolarization-induced facilitation of synaptic transmission at mossy fiber terminals in the hippocampus (Alle and Geiger, 2006). Our present results indicate that depolarizations (e.g., 10–20 mV in amplitude, seconds in duration) similar to those that result in enhancement of synaptic transmission between nearby cortical pyramidal cells results in a significant increase in baseline $[Ca^{2+}]_i$ at presynaptic boutons up to ~200 μm from the soma. As with the depolarization-induced enhancement of intracortical synaptic transmission, the depolarization-induced increase in $[Ca^{2+}]$ was blocked by the addition of EGTA to the recording pipette (Fig. 4). The increases in OGB1 calcium indicator fluorescence were ~5%, although changes as high as 20% in putative presynaptic boutons were sometimes observed (Fig. 2*a*). Given a resting $[Ca^{2+}]_i$ of 100 nM, we suggest that these changes should range from ~10–60 nM (supplemental Fig. S9, available at www.jneurosci.org as supplemental material). At the calyx of Held, increases in synaptic transmission after depolarization exhibit a power law relationship to baseline levels of resting $[Ca^{2+}]_i$ (Awatramani et al., 2005). If intracortical synapses operated in a similar manner, then the 5% (up to 20%) increases in baseline Ca^{2+} observed here may correspond to increases in synaptic transmission of ~14% (up to 65%) (supplemental Fig. S9, available at www.jneurosci.org as supplemental material). Thus, increases in baseline Ca^{2+} may contribute to the average 30% increase in synaptic transmission between nearby cortical pyramidal neurons, particularly for terminals that are within 200 μm of the presynaptic soma.

For both OGB1 and Fluo-5F, we observed that subthreshold depolarization of the membrane potential resulted in an increase

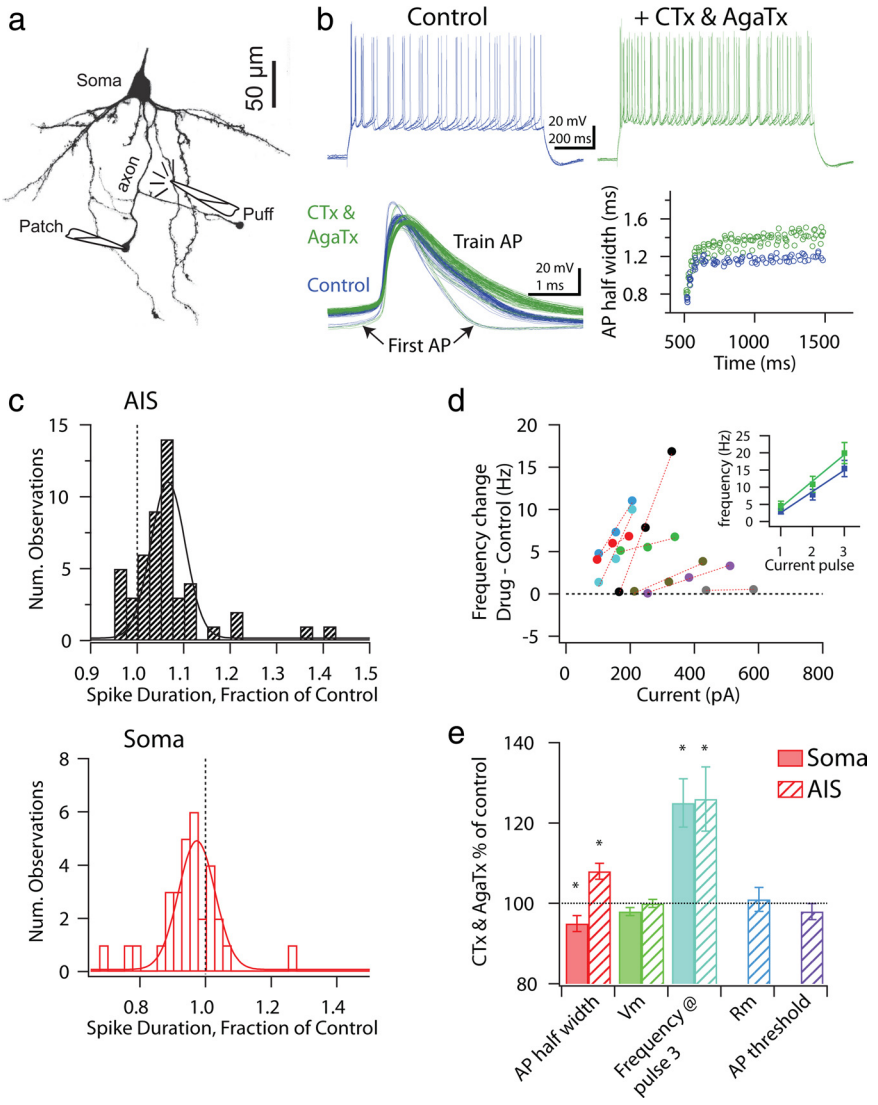

Figure 7. Blocking axonal calcium currents increases axonal spike duration and excitability. ***a***, Illustration of the axonal recording and drug application method. Drugs were applied to the region of the axon initial segment and soma with a puffer pipette within 10–50 μm and oriented toward the AIS. ***b***, Response of the axon to depolarizing current pulse (0.2 nA) before and after local application of ω-conotoxin (15 μM in the pipette) and ω-agatoxin (50 μM in pipette). Blocking P/Q and N channels resulted in an increase in duration of the axonal action potential (AP) as well as an increase in firing frequency. Note spike broadening during the train of action potentials. Block of P/Q and N channels results in spike broadening for all spikes, but particularly for action potentials late in the spike train. ***c***, Plot of relative spike duration (after vs before drug application) in axonal and somatic recordings. All spikes are included for all cells. Block of P/Q and N channels results in spike broadening in the axon, but a decrease in spike duration in the soma. ***d***, Change in firing frequency after application of agatoxin/conotoxin for all three current pulses. Each data set represents a different axonal recording. Inset, Raw data from all AIS recordings. ***e***, Application of agatoxin/conotoxin results in a significant decrease in spike width in the soma, a significant increase in spike width in the axon, an increase firing frequency during current injection for both the axon and soma, and no significant change in baseline membrane potential, input resistance (R_m), or action potential threshold. Error bars indicate SEM. Asterisks indicate significant effects ($p < 0.05$).

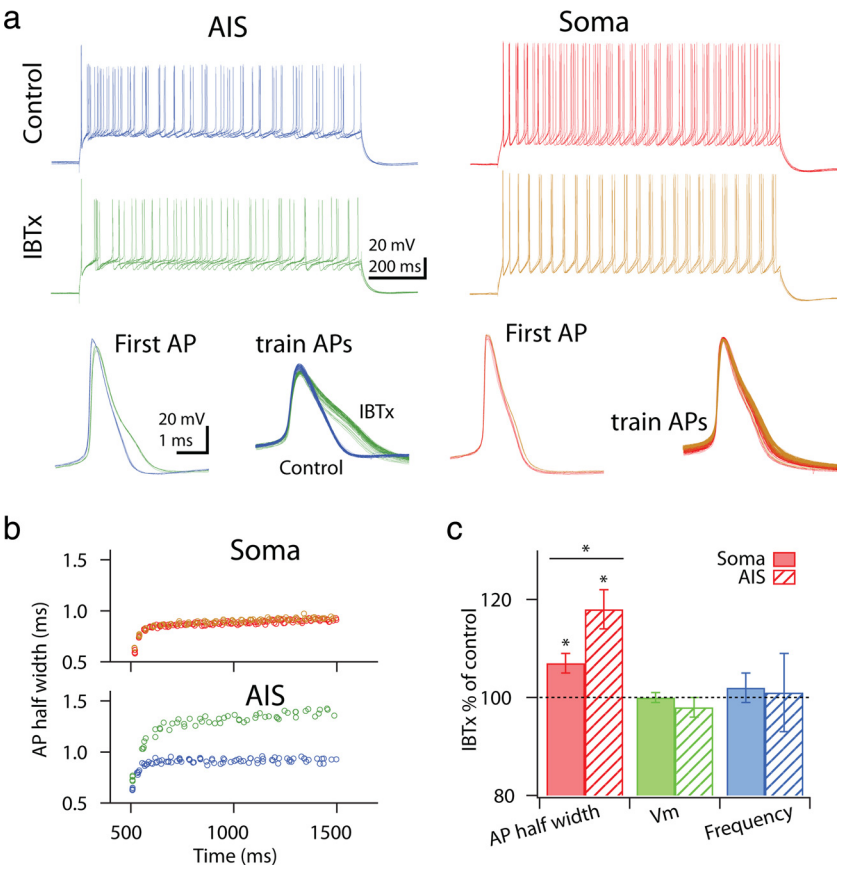

Figure 8. Calcium-activated K^+ currents contribute to spike repolarization in cortical axons. ***a***, Local puffer application of IBTx (10 μM in micropipette), which blocks BK calcium-activated K^+ channels, results in an increase in duration of action potentials in the axon, with a small increase in action potential duration in the soma. The increase in duration of axonal action potentials is associated with the appearance of a "bump" on the falling phase of the axonal spike. ***b***, Plot of the effect of IBTx on spike width in the soma and axon. ***c***, Group data illustrating that IBTx strongly increases spike duration in the axon with a lesser effect in the soma. The baseline membrane potential and frequency of discharge to a current pulse was unaffected. Error bars indicate SEM. Asterisks indicate significant effects ($p < 0.05$).

in absolute peak $[Ca^{2+}]_i$ levels obtained after an action potential in the AIS and nearby synaptic boutons (Fig. 2*d*). In addition, when using Fluo-5F as the calcium indicator dye, we observed that the spike-triggered change in $[Ca^{2+}]_i$ ($\Delta F/R$) was also increased with depolarization of the soma (Fig. 2*e*). This effect was not observed when using OGB1 as the calcium indicator (Fig. 2). Although the origin of this negative observation with OGB1 is unknown, relevant factors include the sublinear response properties of this dye to free $[Ca^{2+}]$ (Yasuda et al., 2004) (but see Higley and Sabatini, 2008), the high background fluorescence of OGB1, as well as the significantly lower $\Delta F/R$ response of OGB1 in response to each action potential compared with Fluo-5F (supplemental Fig. S2, available at www.jneurosci.org as supplemental material).

Increases in spike-triggered Ca^{2+} response in the AIS and nearby presynaptic boutons should increase spike-triggered synaptic transmission and may be a consequence of action potential broadening, because of voltage-dependent inactivation of K^+ channels (Kole et al., 2007; Shu et al., 2007a). Indeed, there is substantial evidence that a change in baseline Ca^{2+} is not the only contributor to increases in synaptic transmission between nearby pyramidal cells. Depolarization of the soma results in a lengthening of the duration of action potentials in the axon through the inactivation of a Kv1-subunit-containing K^+ current, and these changes in spike duration can propagate hundreds of micrometers down the axon (Shu et al., 2006a, 2007a; Kole et al., 2007). Block of Kv1 channels results in axonal action potential broadening, an increase in the average amplitude of intracortical excitatory synaptic transmission, and, at least in some cases, an occlusion of the ability of presynaptic somatic depolarization to further enhance synaptic transmission. The most parsimonious explanation of these results is that depolarization of cortical pyramidal cell somata can result both in an increase in baseline Ca^{2+} levels (and perhaps spike-triggered Ca^{2+} transients) as well as changes in action potential duration, all of which contribute to increases in intracortical synaptic transmission.

Experiments in hippocampal mossy fiber terminals provide evidence for a yet unidentified third mechanism for depolarization-induced enhancement of synaptic transmission. Here, depolarization of the presynaptic terminal results in a rapid (tens of milliseconds) increase in synaptic transmission that is not fully blocked by Ca^{2+} buffering and is not associated with increases in presynaptic action potential duration (Alle and Geiger, 2006). Short-duration (100 ms) depolarization of the soma of granule cells does not increase baseline Ca^{2+} levels or spike-triggered Ca^{2+} responses in mossy fiber boutons (although long-duration depolarizations can increase baseline $[Ca^{2+}]_i$) (Ruiz et al., 2003), and buffering presynaptic Ca^{2+} does not block glutamate- or high-$[K^+]_o$-induced depolarization and enhancement of synaptic transmission at these synapses (Scott et al., 2008). Depolarization of central axons can thus result in a wide variety of modifications of synaptic transmission through a multiple mechanisms that are likely to vary with synapse type and location.

Role of Ca^{2+} currents in AIS function

We observed the prominent presence of both subthreshold and suprathreshold Ca^{2+} signals in the axon initial segment of layer 5 pyramidal cells. Indeed, recent investigations of interneurons in the dorsal cochlear nucleus observed the AIS to contain significant spike-initiated Ca^{2+} signals, which participated strongly in the initiation of bursts of Na^+-dependent action potentials in these neurons. The observation of spike-initiated increases in Ca^{2+} levels in the AIS of cortical pyramidal cells led to the suggestion that similar mechanisms may also occur in the neocortex (Bender and Trussell, 2009). In the dorsal cochlear interneurons, these spike-initiated increases in AIS Ca^{2+} levels were reduced by application of Ni^{2+} and the T-channel antagonist mibefradil as well as the R-channel antagonist SNX482, but not by either ω-agatoxin TK or ω-conotoxin GVIA, leading these authors to hypothesize that this effect is mediated by T- and R-type Ca^{2+} currents (Bender and Trussell, 2009). Our results extend these findings by demonstrating that in addition to a strong spike-triggered increase in Ca^{2+} in the AIS, there is also a significant increase in $[Ca^{2+}]_i$ in this neuronal region after somatic sub-

threshold depolarization. However, our results do not agree with those of Bender and Trussell (2009) on the subtype of Ca^{2+} channel that is likely to mediate this effect in cortical pyramidal neurons. Although Ni^{2+} did have a suppressive effect on both subthreshold and spike-initiated changes in $[Ca^{2+}]_i$, this effect was not replicated with a variety of T-channel antagonists. In contrast, the application of either agatoxin or conotoxin resulted in strong suppressive effects on both the subthreshold and suprathreshold Ca^{2+} responses, suggesting a strong involvement of N and P/Q subtypes of Ca^{2+} channels in the AIS (as well as presynaptic boutons) of cortical pyramidal neurons. These results imply that different cell types contain differing types of Ca^{2+} channels in the AIS, although it is also possible that these differences originated from species or area differences (ferret cortex vs mouse cochlear nucleus) or developmental stages (2- to 3-week-old mouse vs 7- to 9-week-old ferret).

Interestingly, combined block of N and P/Q channels or BK Ca^{2+}-activated K^+ channels (K_{Ca2+}) resulted in an increase in spike duration in the AIS of cortical pyramidal cells, suggesting that the entry of Ca^{2+} through N and P/Q channels facilitates the repolarization of axonal action potentials through the activation of the BK K_{Ca2+} current. Previous studies have found that the block of BK K_{Ca2+} channels results in a small increase in duration of somatic action potentials in the neocortex (Sun et al., 2003; Benhassine and Berger, 2009) and hippocampus (Shao et al., 1999; Gu et al., 2007). Our results include the novel demonstration that BK channels contribute even more strongly to spike repolarization in the AIS than in the soma of layer 5 pyramidal neurons, and thus to controlling the input–output properties of this important region for neuronal excitability. Calcium (N and P/Q) as well as BK channels are prominent in intracortical synaptic terminals, and similar mechanisms for the control of intracortical synaptic transmission may be at play here (Hu et al., 2001; Raffaelli et al., 2004).

Reduction of BK channel activation is unlikely to mediate the increase in excitability observed in cortical neurons after the block of N and P/Q Ca^{2+} channels that we observed, since BK channels depend on combined strong depolarization as well as micromolar increases in $[Ca^{2+}]_i$ (Womack and Khodakhah, 2002). Indeed, we observed that the block of BK channels did not result in a significant increase in the response of cortical pyramidal neurons to depolarizing current pulses. We hypothesize that the increase in neuronal excitability observed after block of N and P/Q Ca^{2+} channels results from a reduction in another K_{Ca2+}, perhaps of either the apamin-sensitive or apamin-insensitive SK type (Sah, 1996).

Our results indicate that N and P/Q calcium channels make important contributions to the physiological properties of both the axon initial segment as well as presynaptic boutons of intracortical axons. P/Q and N calcium currents are intimately involved not only in the repolarization of action potentials, but also in the adjustment of the baseline levels of Ca^{2+} that slowly track the membrane potential of the soma (and axon). Through these changes in resting and spike-trigger evoked calcium entry, axonal calcium currents may make important contributions to intracortical excitability, network processing, and neuronal plasticity. Indeed, it was shown recently that Na^+ channel localization in the AIS is experience dependent and that this effect operates through the activation of Ca^{2+} channels (Grubb and Burrone, 2010). Finally, mutations in N and P/Q channels may underlie various neurological disorders including migraine and ataxia (Catterall et al., 2008; Urbano et al., 2008). The possibility that the important location of these disruptions is either the AIS or presynaptic terminals remains to be investigated.

References

Alle H, Geiger JR (2006) Combined analog and action potential coding in hippocampal mossy fibers. Science 311:1290–1293.

Arroyo G, Aldea M, Fuentealba J, Albillos A, Garcia AG (2003) SNX482 selectively blocks P/Q Ca2+ channels and delays the inactivation of Na+ channels of chromaffin cells. Eur J Pharmacol 475:11–18.

Astman N, Gutnick MJ, Fleidervish IA (2006) Persistent sodium current in layer 5 neocortical neurons is primarily generated in the proximal axon. J Neurosci 26:3465–3473.

Awatramani GB, Price GD, Trussell LO (2005) Modulation of transmitter release by presynaptic resting potential and background calcium levels. Neuron 48:109–121.

Bender KJ, Trussell LO (2009) Axon initial segment Ca2+ channels influence action potential generation and timing. Neuron 61:259–271.

Benhassine N, Berger T (2009) Large-conductance calcium-dependent potassium channels prevent dendritic excitability in neocortical pyramidal neurons. Pflugers Arch 457:1133–1145.

Binzegger T, Douglas RJ, Martin KA (2004) A quantitative map of the circuit of cat primary visual cortex. J Neurosci 24:8441–8453.

Binzegger T, Douglas RJ, Martin KA (2005) Axons in cat visual cortex are topologically self-similar. Cereb Cortex 15:152–165.

Brenowitz SD, Regehr WG (2007) Reliability and heterogeneity of calcium signaling at single presynaptic boutons of cerebellar granule cells. J Neurosci 27:7888–7898.

Catterall WA, Dib-Hajj S, Meisler MH, Pietrobon D (2008) Inherited neuronal ion channelopathies: new windows on complex neurological diseases. J Neurosci 28:11768–11777.

Currie KP, Fox AP (1997) Comparison of N- and P/Q-type voltage-gated calcium channel current inhibition. J Neurosci 17:4570–4579.

Debanne D (2004) Information processing in the axon. Nat Rev Neurosci 5:304–316.

Devaux J, Alcaraz G, Grinspan J, Bennett V, Joho R, Crest M, Scherer SS (2003) Kv3.1b is a novel component of CNS nodes. J Neurosci 23:4509–4518.

Devaux JJ, Kleopa KA, Cooper EC, Scherer SS (2004) KCNQ2 is a nodal K^+ channel. J Neurosci 24:1236–1244.

Galvez A, Gimenez-Gallego G, Reuben JP, Roy-Contancin L, Feigenbaum P, Kaczorowski GJ, Garcia ML (1990) Purification and characterization of a unique, potent, peptidyl probe for the high conductance calcium-activated potassium channel from venom of the scorpion *Buthus tamulus*. J Biol Chem 265:11083–11090.

Grubb MS, Burrone J (2010) Activity-dependent relocation of the axon initial segment fine-tunes neuronal excitability. Nature 465:1070–1074.

Gu N, Vervaeke K, Storm JF (2007) BK potassium channels facilitate high-frequency firing and cause early spike frequency adaptation in rat CA1 hippocampal pyramidal cells. J Physiol 580:859–882.

Higley MJ, Sabatini BL (2008) Calcium signaling in dendrites and spines: practical and functional considerations. Neuron 59:902–913.

Hu H, Shao LR, Chavoshy S, Gu N, Trieb M, Behrens R, Laake P, Pongs O, Knaus HG, Ottersen OP, Storm JF (2001) Presynaptic Ca^{2+}-activated K^+ channels in glutamatergic hippocampal terminals and their role in spike repolarization and regulation of transmitter release. J Neurosci 21:9585–9597.

Hu W, Tian C, Li T, Yang M, Hou H, Shu Y (2009) Distinct contributions of Na(v)1.6 and Na(v)1.2 in action potential initiation and backpropagation. Nat Neurosci 12:996–1002.

Huang L, Keyser BM, Tagmose TM, Hansen JB, Taylor JT, Zhuang H, Zhang M, Ragsdale DS, Li M (2004) NNC 55–0396 [(1*S*,2*S*)-2-(2-(*N*-[(3-benzimidazol-2-yl)propyl]-*N*-methylamino)ethyl)-6-fluoro-1,2,3,4-tetrahydro-1-isopropyl-2-naphtyl cyclopropanecarboxylate dihydrochloride]: a new selective inhibitor of T-type calcium channels. J Pharmacol Exp Ther 309:193–199.

Inda MC, DeFelipe J, Munoz A (2006) Voltage-gated ion channels in the axon initial segment of human cortical pyramidal cells and their relationship with chandelier cells. Proc Natl Acad Sci U S A 103:2920–2925.

Koester HJ, Sakmann B (2000) Calcium dynamics associated with action potentials in single nerve terminals of pyramidal cells in layer 2/3 of the young rat neocortex. J Physiol 529:625–646.

Kole MH, Letzkus JJ, Stuart GJ (2007) Axon initial segment Kv1 channels

control axonal action potential waveform and synaptic efficacy. Neuron 55:633–647.
Kole MH, Ilschner SU, Kampa BM, Williams SR, Ruben PC, Stuart GJ (2008) Action potential generation requires a high sodium channel density in the axon initial segment. Nat Neurosci 11:178–186.
Lopez I, Ishiyama G, Ishiyama A, Jen JC, Liu F, Baloh RW (1999) Differential subcellular immunolocalization of voltage-gated calcium channel alpha1 subunits in the chinchilla cristae ampullaris. Neuroscience 92: 773–782.
Lorincz A, Nusser Z (2008) Cell-type-dependent molecular composition of the axon initial segment. J Neurosci 28:14329–14340.
Magee JC, Johnston D (1995) Characterization of single voltage-gated Na^+ and Ca^{2+} channels in apical dendrites of rat CA1 pyramidal neurons. J Physiol 487:67–90.
Magee JC, Christofi G, Miyakawa H, Christie B, Lasser-Ross N, Johnston D (1995) Subthreshold synaptic activation of voltage-gated Ca^{2+} channels mediates a localized Ca^{2+} influx into the dendrites of hippocampal pyramidal neurons. J Neurophysiol 74:1335–1342.
Majewska A, Yiu G, Yuste R (2000) A custom-made two-photon microscope and deconvolution system. Pflugers Arch 441:398–408.
Maravall M, Mainen ZF, Sabatini BL, Svoboda K (2000) Estimating intracellular calcium concentrations and buffering without wavelength ratioing. Biophys J 78:2655–2667.
Martin RL, Lee JH, Cribbs LL, Perez-Reyes E, Hanck DA (2000) Mibefradil block of cloned T-type calcium channels. J Pharmacol Exp Ther 295:302–308.
Ogiwara I, Miyamoto H, Morita N, Atapour N, Mazaki E, Inoue I, Takeuchi T, Itohara S, Yanagawa Y, Obata K, Furuichi T, Hensch TK, Yamakawa K (2007) Na(v)1.1 localizes to axons of parvalbumin-positive inhibitory interneurons: a circuit basis for epileptic seizures in mice carrying an Scn1a gene mutation. J Neurosci 27:5903–5914.
Palmer LM, Stuart GJ (2006) Site of action potential initiation in layer 5 pyramidal neurons. J Neurosci 26:1854–1863.
Pan Z, Kao T, Horvath Z, Lemos J, Sul JY, Cranstoun SD, Bennett V, Scherer SS, Cooper EC (2006) A common ankyrin-G-based mechanism retains KCNQ and NaV channels at electrically active domains of the axon. J Neurosci 26:2599–2613.
Raffaelli G, Saviane C, Mohajerani MH, Pedarzani P, Cherubini E (2004) BK potassium channels control transmitter release at CA3-CA3 synapses in the rat hippocampus. J Physiol 557:147–157.
Ruiz A, Fabian-Fine R, Scott R, Walker MC, Rusakov DA, Kullmann DM (2003) GABAA receptors at hippocampal mossy fibers. Neuron 39:961–973.
Rusakov DA (2006) Ca^{2+}-dependent mechanisms of presynaptic control at central synapses. Neuroscientist 12:317–326.
Sah P (1996) Ca(2+)-activated K+ currents in neurones: types, physiological roles and modulation. Trends Neurosci 19:150–154.
Scott R, Rusakov DA (2006) Main determinants of presynaptic Ca^{2+} dynamics at individual mossy fiber-CA3 pyramidal cell synapses. J Neurosci 26:7071–7081.
Scott R, Ruiz A, Henneberger C, Kullmann DM, Rusakov DA (2008) Analog modulation of mossy fiber transmission is uncoupled from changes in presynaptic Ca^{2+}. J Neurosci 28:7765–7773.
Shao LR, Halvorsrud R, Borg-Graham L, Storm JF (1999) The role of BK-type Ca^{2+}-dependent K^+ channels in spike broadening during repetitive firing in rat hippocampal pyramidal cells. J Physiol 521:135–146.
Shu Y, Hasenstaub A, Duque A, Yu Y, McCormick DA (2006a) Modulation of intracortical synaptic potentials by presynaptic somatic membrane potential. Nature 441:761–765.
Shu Y, Hasenstaub A, Duque A, Yu Y, McCormick DA (2006b) Modulation of intracortical synaptic potentials by presynaptic somatic membrane potential. Nature 441:761–765.
Shu Y, Yu Y, Yang J, McCormick DA (2007a) Selective control of cortical axonal spikes by a slowly inactivating K^+ current. Proc Natl Acad Sci U S A 104:11453–11458.
Shu Y, Duque A, Yu Y, Haider B, McCormick DA (2007b) Properties of action-potential initiation in neocortical pyramidal cells: evidence from whole cell axon recordings. J Neurophysiol 97:746–760.
Stuart G, Spruston N, Sakmann B, Hausser M (1997) Action potential initiation and backpropagation in neurons of the mammalian CNS. Trends Neurosci 20:125–131.
Sun X, Gu XQ, Haddad GG (2003) Calcium influx via L- and N-type calcium channels activates a transient large-conductance Ca^{2+}-activated K^+ current in mouse neocortical pyramidal neurons. J Neurosci 23:3639–3648.
Traboulsie A, Chemin J, Kupfer E, Nargeot J, Lory P (2006) T-type calcium channels are inhibited by fluoxetine and its metabolite norfluoxetine. Mol Pharmacol 69:1963–1968.
Urbano FJ, Pagani MR, Uchitel OD (2008) Calcium channels, neuromuscular synaptic transmission and neurological diseases. J Neuroimmunol 201–202:136–144.
Vervaeke K, Gu N, Agdestein C, Hu H, Storm JF (2006) Kv7/KCNQ/M-channels in rat glutamatergic hippocampal axons and their role in regulation of excitability and transmitter release. J Physiol 576:235–256.
Womack MD, Khodakhah K (2002) Characterization of large conductance Ca^{2+}-activated K^+ channels in cerebellar Purkinje neurons. Eur J Neurosci 16:1214–1222.
Woodruff ML, Sampath AP, Matthews HR, Krasnoperova NV, Lem J, Fain GL (2002) Measurement of cytoplasmic calcium concentration in the rods of wild-type and transducin knock-out mice. J Physiol 542:843–854.
Yasuda R, Nimchinsky EA, Scheuss V, Pologruto TA, Oertner TG, Sabatini BL, Svoboda K (2004) Imaging calcium concentration dynamics in small neuronal compartments. Sci STKE 219:p.p15.
Yu Y, Shu Y, McCormick DA (2008) Cortical action potential backpropagation explains spike threshold variability and rapid-onset kinetics. J Neurosci 28:7260–7272.
Zamponi GW, Bourinet E, Snutch TP (1996) Nickel block of a family of neuronal calcium channels: subtype- and subunit-dependent action at multiple sites. J Membr Biol 151:77–90.